

# Relativistic models for quasielastic ( $e, e'$ ) at large momentum transfers

Hungchong Kim\* and C. J. Horowitz†

*Nuclear Theory Center and Department of Physics, Indiana University, Bloomington, Indiana 47408*

M. R. Frank‡

*Institute for Nuclear Theory, University of Washington, Seattle, Washington 98195*

(Received 3 October 1994)

Inclusive quasielastic response functions are calculated for electron scattering in a relativistic model including momentum dependent scalar and vector mean fields. The momentum dependence of the mean fields is taken from Dirac optical fits to proton nucleus scattering and is important in describing data at momentum transfers of 1 GeV/c or larger. Our simple model is applicable for quasielastic scattering over a large range of momentum transfers.

PACS number(s): 13.60.Fz, 25.30.Fj, 24.10.Jv

## I. INTRODUCTION

There is growing interest in quasielastic electron scattering experiments with momentum transfers of order 1 GeV/c or larger. Clearly these require a relativistic treatment. Indeed, there have been many relativistic mean field and random phase approximation (RPA) calculations of quasielastic scattering [1-3]. These calculations often have large scalar  $S$  and vector  $V$  mean fields which shift the mass of a nucleon from  $M$  to  $M^*$ ,

$$M^* = M + S. \quad (1)$$

This changes the position of the quasielastic peak from  $\omega \approx \mathbf{q}^2/2M$  (with  $\mathbf{q}$  the momentum and  $\omega$  the energy transfer) to

$$\omega \approx \sqrt{\mathbf{q}^2 + (M^*)^2} - M^*. \quad (2)$$

This change agrees well with the "binding-energy" shift seen in a variety of experiments at moderate momentum transfers  $|\mathbf{q}| \leq 600$  MeV/c.

However, Eq. (2) predicts very large shifts for momentum transfers of order 1000 MeV/c or larger. Such large shifts are not seen in the data [4]. One would like to understand this limitation and develop a simple relativistic mean field model that is applicable over a broad range of momentum transfers. Indeed, most of the relativistic models assume the self-energies or mean fields ( $S, V$ ) are independent of energy or momentum. This approximation is probably good at low momentum transfers but fails as the momentum transfer increases.

Dirac optical model fits to proton-nucleus elastic scattering [5] produce scalar and vector optical potentials

which have much less energy dependence than the non-relativistic mean field. When the Dirac equation is reduced to a Schrödinger-like form the effective nonrelativistic mean field is [6]

$$U_{\text{opt}} = S + \frac{E}{M}V + \frac{1}{2M}(S^2 - V^2). \quad (3)$$

Here  $E$  is the total energy of the nucleon ( $T_{\text{lab}} + M$ ). The linear energy dependence for  $U_{\text{opt}}$  implied by Eq. (3) agrees well with data for  $T_{\text{lab}}$  of order 200-300 MeV or less. However, Eq. (3) (with constant  $S, V$ ) greatly overpredicts the energy-dependence of  $U_{\text{opt}}$  above 300 MeV. As a result Dirac optical fits need *energy-dependent*  $S$  and  $V$  in order to reproduce elastic data at higher energies. One such fit is shown in Fig. 1.

The magnitudes of  $S$  and  $V$  decrease with energy. This

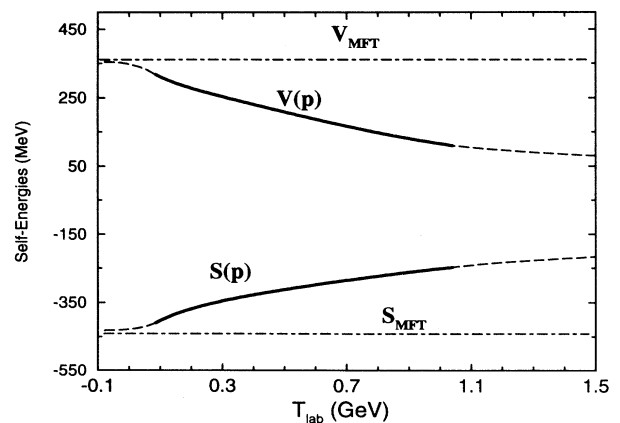


FIG. 1. Scalar  $S$  and vector  $V$  mean fields versus laboratory kinetic energy  $T_{\text{lab}}$ . Solid lines are real parts of a Dirac optical model fit to  $p$ - $^{40}\text{Ca}$  elastic scattering [5] while dot-dashed lines are the constant relativistic mean field values [10]. The dashed lines are extrapolations as described in the text.

\*Electronic address: hung@iucf.indiana.edu

†Electronic address: charlie@iucf.indiana.edu

‡Electronic address: frank@ben.npl.washington.edu

trend is also reproduced in relativistic Brueckner calculations [7,8]. In this paper we use such momentum- or energy-dependent potentials to calculate inclusive quasielastic electron scattering over a large range of momentum transfers. Results for a simplified form of momentum-dependent potentials were presented in an earlier paper [9]. Our formalism is described in Sec. II. Results for  $^{56}\text{Fe}$  and  $^{40}\text{Ca}$  are given in Sec. III. This section also discusses current conservation. We summarize in Sec. IV.

## II. FORMALISM

The inclusive ( $e, e'$ ) cross section for excitation energy  $\omega$  and three-momentum transfer  $\mathbf{q}$  is

$$\frac{d^2\sigma}{d\Omega dE} = \sigma_M \left[ \frac{Q^4}{\mathbf{q}^4} R_L(\mathbf{q}, \omega) + \left( \frac{Q^2}{2\mathbf{q}^2} + \tan^2 \frac{\theta}{2} \right) R_T(\mathbf{q}, \omega) \right], \quad (4)$$

with the Mott cross section  $\sigma_M = \alpha^2 \cos^2(\theta/2) / 4E^2 \sin^2(\theta/2)$ . Here  $Q^2 = -q_\mu^2 = \mathbf{q}^2 - \omega^2$  and  $\theta$  is the scattering angle. The longitudinal  $R_L$  and transverse  $R_T$  response functions are calculated in a local density approximation from nuclear matter at a density  $\rho = 2k_F^3/3\pi^2$ ,

$$R_L = -\frac{2}{\pi\rho} \text{Im}(Z\Pi_{00}^p + N\Pi_{00}^n), \quad (5)$$

$$R_T = -\frac{4}{\pi\rho} \text{Im}(Z\Pi_{22}^p + N\Pi_{22}^n), \quad (6)$$

for a target with  $Z$  protons and  $N$  neutrons. (Note that  $\mathbf{q}$  is assumed to be along the  $\hat{z}$  axis, and so the subscript 22 refers to a transverse direction.)

The polarization  $\Pi$  is calculated with the nucleon Green's function  $G(p)$  and the electromagnetic vertex  $\Gamma$ ,

$$\Pi_{\mu\nu}^i(q, \omega) = -i \int \frac{d^4p}{(2\pi)^4} \text{Tr}[G(p+q)\Gamma_\mu^i G(p)\Gamma_\nu^i], \quad (7)$$

for  $i = p$  (proton) or  $n$  (neutron). We assume that the electromagnetic vertex has the simple form

$$\Gamma_\mu^i = F_1^i \gamma_\mu + F_2^i \frac{i\sigma_{\mu\nu} q^\nu}{2M} \quad (8)$$

even for off-shell nucleons in the medium.

We calculate  $G$  in a mean field approximation. The nucleon self-energy is assumed to be

$$\Sigma = \gamma_0 V(\mathbf{p}) + S(\mathbf{p}), \quad (9)$$

where  $S$  and  $V$  are taken from a Dirac optical fit at the self-consistent energy  $E_{\mathbf{p}}$ ,

$$E_{\mathbf{p}} = \sqrt{\mathbf{p}^2 + [M + S(\mathbf{p})]^2} + V(\mathbf{p}). \quad (10)$$

The Green's function for a Fermi momentum  $k_F$  is

$$G(p) = (p_\mu^* \gamma^\mu + M_{\mathbf{p}}^*) \left[ \frac{1}{p^{*2} - M_{\mathbf{p}}^{*2} + i\epsilon} + \frac{i\pi}{E_{\mathbf{p}}^*} \delta(p_0 - E_{\mathbf{p}}) \Theta(k_F - |\mathbf{p}|) \right]. \quad (11)$$

Here,

$$p_\mu^* = \{p_0 - V(\mathbf{p}), \mathbf{p}\}, \quad (12)$$

$$M_{\mathbf{p}}^* = M + S(\mathbf{p}), \quad (13)$$

and  $E_{\mathbf{p}}^* = \sqrt{\mathbf{p}^2 + M_{\mathbf{p}}^{*2}}$ .

We use  $S(\mathbf{p})$  and  $V(\mathbf{p})$  from the real parts of an optical fit to  $p$ - $^{40}\text{Ca}$  elastic scattering. This fit reproduces experimental data from 21 MeV up to a laboratory kinetic energy of 1.04 GeV [5]. For energies below 21 MeV we interpolate between this fit and the mean field approximation to the Walecka model values of [10]

$$V_{\text{MFT}} = 354 \text{ MeV}, \quad (14)$$

$$S_{\text{MFT}} = -431 \text{ MeV}. \quad (15)$$

For energies greater than 1.04 GeV we use the smooth extrapolation shown in Fig. 1. (However, results we present are not sensitive to this region.) Note that the optical fit has imaginary parts for  $S$  and  $V$  which we ignore. It remains to investigate the effects of these complex potentials.

We use the fit potentials at the center of  $^{40}\text{Ca}$ . However, we scale these results by  $\alpha$ ,

$$\alpha = \frac{\int d^3r \rho(r)^2}{\rho_0 \int d^3r \rho(r)} = (230/257)^3, \quad (16)$$

to represent an average over the nuclear volume. Here  $\rho(r)$  is taken from a relativistic mean field calculation of  $^{40}\text{Ca}$  [10]. We assume the potentials scale with the density and then use a Fermi momentum of

$$k_F = 230 \text{ MeV}/c, \quad (17)$$

in our calculations rather than a typical nuclear matter value  $k_F^0 \approx 257 \text{ MeV}/c$  with  $\rho_0 = 2k_F^0{}^3/3\pi^2$ . This represents an average over the central and low density surface regions.

The polarizations in Eq. (7) are calculated numerically using the Green's function in Eq. (11) as discussed in the Appendix. The parameters of the calculation are the Fermi momentum  $k_F$ ,  $\alpha$ , and the two functions  $S(\mathbf{p})$  and  $V(\mathbf{p})$  from the Dirac optical fit. This yields a simple relativistic impulse approximation that will be applied to data over a large range of momentum transfers in the next section.

## III. RESULTS

In this section we present results for three calculations. The first is a free Fermi gas with  $S(\mathbf{p}) = V(\mathbf{p}) = 0$ . The second is the mean field theory (MFT) with momentum-

independent  $V$  and  $S$  given by Eqs. (14) and (15) [scaled by the  $\alpha$  of Eq. (16)]. Finally, we consider momentum-dependent  $S(\mathbf{p})$  and  $V(\mathbf{p})$ .

The longitudinal response for  $^{56}\text{Fe}$  at  $|\mathbf{q}| = 550 \text{ MeV}/c$  is shown in Fig. 2. The free Fermi gas somewhat underestimates the average excitation energy of the response. This is better described by either the full momentum-dependent calculation or the MFT. Indeed at this relatively low excitation energy of about 200 MeV there are not too large differences between the momentum-dependent  $S(\mathbf{p})$ ,  $V(\mathbf{p})$  and the MFT potentials. Therefore, either the MFT or the momentum-dependent calculation can describe the average excitation energy of low momentum transfer data.

We have used a simple local density approximation. This is expected to reproduce qualitatively the position of the quasielastic peak. Full relativistic finite nucleus calculations (for momentum-independent potentials) [3] agree well with the local density peak positions and do a good job of reproducing the detailed shape of the response. Note that the area under the longitudinal response is controversial. It is subject to systematic experimental errors and Coulomb distortion corrections. However, there is general agreement that (near this momentum transfer) there is a substantial binding-energy shift compared to a free Fermi gas. This is seen either in separated longitudinal and transverse responses or in unseparated cross sections.

Next, Fig. 3 shows the longitudinal response at a momentum transfer of  $|\mathbf{q}| = 1.14 \text{ GeV}/c$ . At this momentum transfer the MFT response is at substantially too high an excitation energy. In contrast, either the momentum-dependent or the free Fermi gas calculation provides a reasonable description of the position of the

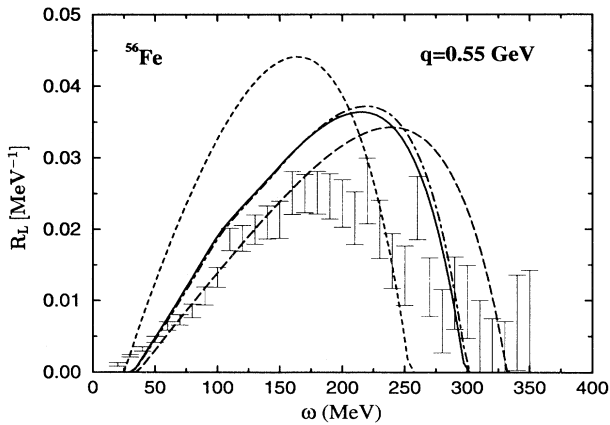


FIG. 2. Longitudinal response function for  $^{56}\text{Fe}$  at a momentum transfer of  $q=550 \text{ MeV}/c$  versus excitation energy  $\omega$ . The solid curve is the full momentum-dependent calculation including the vertex correction from Eq. (21) while the dot-dashed curve omits this vertex correction. The short-dashed curve is the response for a free Fermi gas while the dashed curve is the response assuming constant relativistic mean field theory self-energies. The data are from Ref. [13].

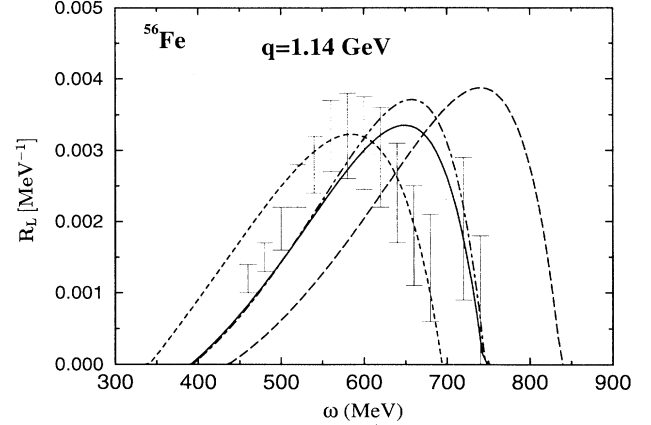


FIG. 3. Longitudinal response for  $^{56}\text{Fe}$  at a momentum transfer of  $q=1.14 \text{ GeV}/c$ . See the caption to Fig. 2. The data are from Ref. [4].

quasielastic peak. Thus the reduction of  $S(\mathbf{p})$  and  $V(\mathbf{p})$  with increasing energy or momentum (as shown in Fig. 1) corrects (at least in large measure) the tendency for the MFT to overpredict the binding energy shift. At still higher momentum transfers, we expect small differences between the momentum-dependent calculation and a free Fermi gas because  $S(\mathbf{p})$  and  $V(\mathbf{p})$  continue to decrease.

The transverse response for  $^{40}\text{Ca}$  is shown in Fig. 4 for  $|\mathbf{q}| = 550 \text{ MeV}/c$ . Again, at this  $q$  the MFT and momentum-dependent calculations are similar. Note that there is substantial extra strength in the transverse response at high excitation energies from meson exchange currents and delta production; see for example [11]. These are not contained in our simple model.

Note that a free Fermi gas reproduces the peak position well at high  $q$ . However, there is no theoretical motivation for simply ignoring the mean fields which are known to be present. Furthermore, a free Fermi gas will

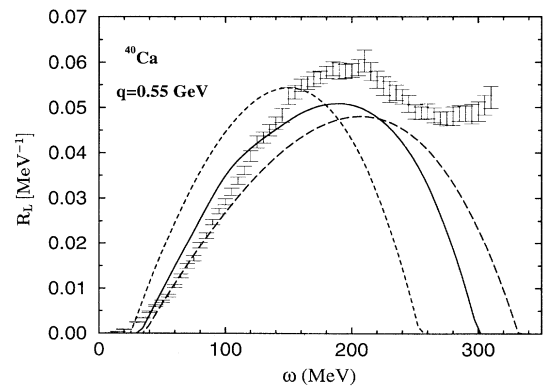


FIG. 4. Transverse response for  $^{40}\text{Ca}$  at a momentum transfer of  $q=550 \text{ MeV}/c$ . The solid curve is the full momentum-dependent calculation while the short-dashed is a free Fermi gas and the dashed is for constant relativistic mean field theory self-energies. The data are from Ref. [12].

fail at low  $q$  where it is generally believed one needs a binding-energy shift. Thus, we think, the only theoretically consistent model is one which includes mean fields and takes into account their momentum dependence.

Alternatively, some nonrelativistic models simply assume a momentum-independent excitation energy shift equal to the average binding energy of a nucleon. This works reasonably well at low  $q$  and possibly could be extended to high  $q$  by using some form of relativistic kinematics. However, there is no theoretical justification for this prescription. Strictly speaking one would have to assume an energy-dependent potential which is big for bound states and then goes rapidly to zero for positive energies. This is unrealistic. Thus, we believe that a theoretically consistent description will have to address explicitly the momentum or energy dependence of the mean fields.

We now discuss current conservation. The full electromagnetic vertex should satisfy the Ward-Takahashi identity

$$q_\mu \Gamma_{\text{full}}^\mu = G^{-1}(p+q) - G^{-1}(p) . \quad (18)$$

This is no longer true for the vertex  $\Gamma^\mu$ , of Eq. (8), given that  $G$  is calculated with momentum-dependent potentials [and that Eq. (8) has form factors]. Clearly we must add a vertex correction. However, there is no unique way to calculate this correction without detailed knowledge of the processes included in  $S(\mathbf{p})$  and  $V(\mathbf{p})$  and in  $F_1$  and  $F_2$ .

Instead, we add a very minimal vertex correction so that not Eq. (18) but at least current conservation is satisfied,

$$\bar{U}(S(\mathbf{p}), V(\mathbf{p})) q_\mu \Gamma_{\text{full}}^\mu U(S(\mathbf{p}), V(\mathbf{p})) = 0 . \quad (19)$$

Here, the spinors  $U$  satisfy a Dirac equation with  $S, V$  and

$$\Gamma_{\text{full}}^\mu = \Gamma^\mu + \Delta\Gamma^\mu . \quad (20)$$

We choose

$$\begin{aligned} \Delta\Gamma^{\mu i} = q^\mu \frac{F_1^i(q_\lambda^2)}{q_\lambda^2} [S(\mathbf{p} + \mathbf{q}) + \gamma_0 V(\mathbf{p} + \mathbf{q}) \\ - S(\mathbf{p}) - \gamma_0 V(\mathbf{p})] . \end{aligned} \quad (21)$$

This simple prescription ensures

$$q^\mu \Pi_{\mu\nu} = \Pi_{\mu\nu} q^\nu = 0 . \quad (22)$$

Calculations using Eqs. (20) and (21) are shown in Figs. 2, 3 and are only slightly smaller than calculations with  $\Delta\Gamma^\mu = 0$ .<sup>1</sup> Therefore, we do not expect large er-

<sup>1</sup>Note that Eq. (21) does not contribute to  $R_L$  when contracted with the conserved electron current. However, Eqs. (4) and (5) assumed current conservation. One gets a different answer for  $R_L$  from Eq. (5) if one sets  $\Delta\Gamma^\mu = 0$  because in this case the current is not conserved.

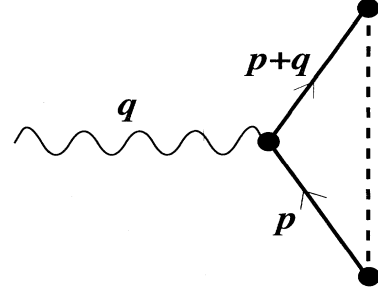


FIG. 5. Vertex correction in a relativistic Hartree-Fock approximation. The nucleon line is solid while the dashed line is an exchanged meson and the wavy line a photon.

rors from our (slight) violation of current conservation. However, Eq. (21) is nonunique and this point deserves further study; see below.

#### IV. SUMMARY AND CONCLUSIONS

There have been many relativistic mean field calculations for inclusive quasielastic electron scattering. Ironically, although these do a reasonable job at low to moderate momentum transfers, many of these relativistic calculations are not appropriate for momentum transfers near 1 GeV/c or above. This is because they assume the mean fields are independent of momentum or energy. As a result they predict too large a binding energy shift in the position of the quasielastic peak.

Instead, we assume a simple model where the momentum dependence of the scalar and vector mean fields are taken from an optical model fit to  $p$ -<sup>40</sup>Ca elastic scattering. The inclusive response is calculated in a relativistic impulse approximation. Reasonable predictions are made for the position of the quasielastic peak at both low and high  $q$ . Therefore, the model can be used over a large range of momentum transfers.

Our calculations are for nuclear matter in a local density approximation. We expect this to qualitatively reproduce the position of the quasielastic peak but not its detailed shape. One should repeat the calculations in a full finite nucleus formalism, such as from Ref. [3], using energy-dependent potentials.

We have only briefly mentioned vertex corrections. These are needed for current conservation in momentum-dependent mean fields. Future work should calculate the vertex correction in a full microscopic model. For example, one can choose a (somewhat unusual) set of meson couplings (including nonlinear self-couplings) so that a relativistic Hartree-Fock (HF) calculation approximately reproduces the momentum dependence of the mean fields. This allows the vertex correction to be calculated explicitly from the diagram in Fig. 5.

#### ACKNOWLEDGMENTS

We would like to thank B. C. Clark for providing us a computer code “global” which generates the nuclear op-

tical potentials. This research was supported by U.S. Department of Energy under Grants No. DE-FG02-87ER-40365 and DE-FG06-90ER-40561.

### APPENDIX

Here we summarize the calculation of imaginary part of the polarization  $\Pi^{\mu\nu}$ . The Green's function of Eq. (11) can be written in three parts: (1) the propagation of an antinucleon in the Dirac sea, the propagation of a (2) hole inside, and a (3) particle outside of the Fermi sea. Since vacuum polarization does not contribute to the imaginary part for the spacelike  $q_\mu$ , the propagation of antinucleons can be dropped and the Green's function [Eq. (11)] written

$$G(p) = \frac{p_\mu^* \gamma^\mu + M_{\mathbf{p}}^*}{2E_{\mathbf{p}}^*} \left[ \frac{\Theta(k_F - |\mathbf{p}|)}{p_0 - E_{\mathbf{p}} - i\epsilon} + \frac{\Theta(|\mathbf{p}| - k_F)}{p_0 - E_{\mathbf{p}} + i\epsilon} \right]. \quad (\text{A1})$$

Using this Green's function, it is straightforward to integrate over  $p_0$  and the imaginary part of the polarization becomes

$$\text{Im } \Pi^{\mu\nu} = - \int \frac{\mathbf{p}^2 d|\mathbf{p}| d\cos\theta}{4\pi E_{\mathbf{p}}^* E_{\mathbf{p}+\mathbf{q}}^*} \Theta(|\mathbf{p} + \mathbf{q}| - k_F) \Theta(k_F - |\mathbf{p}|) \times \delta(E_{\mathbf{p}+\mathbf{q}} - E_{\mathbf{p}} - q_0) [T_1^{\mu\nu} + T_2^{\mu\nu} + T_3^{\mu\nu}], \quad (\text{A2})$$

where  $\cos\theta$  is the angle between  $\mathbf{p}$  and  $\mathbf{q}$ . Here  $T_1$ ,  $T_2$ , and  $T_3$  are from the trace of Dirac matrices,

$$T_1^{\mu\nu} = F_1^{i2} [(p+q)^{* \mu} p^{*\nu} - p^* \cdot (p+q)^* g^{\mu\nu} + p^{*\mu} (p+q)^{* \nu} + M_{\mathbf{p}}^* M_{\mathbf{p}+\mathbf{q}}^* g^{\mu\nu}], \quad (\text{A3})$$

$$T_2^{\mu\nu} = \frac{F_1^i F_2^i}{2M} \left[ M_{\mathbf{p}}^* [(p+q)^* \cdot q g^{\mu\nu} - (p+q)^{* \mu} q^\nu] + M_{\mathbf{p}+\mathbf{q}}^* [p^{*\mu} q^\nu - p^* \cdot q g^{\mu\nu}] \right], \quad (\text{A4})$$

$$T_3^{\mu\nu} = \frac{F_2^{i2}}{4M^2} \left\{ [M_{\mathbf{p}+\mathbf{q}}^* M_{\mathbf{p}}^* + p^* \cdot (p+q)^*] (g^{\mu\nu} q_\mu^2 - q^\mu q^\nu) + p^* \cdot q [(p+q)^{* \mu} q^\nu + (p+q)^{* \nu} q^\mu] - q_\mu^2 [(p+q)^{* \mu} p^{*\nu} + (p+q)^{* \nu} p^{*\mu}] + (p+q)^* \cdot q [q^\mu p^{*\nu} + q^\nu p^{*\mu}] - 2p^* \cdot q (p+q)^* \cdot q g^{\mu\nu} \right\}, \quad (\text{A5})$$

with  $p^{*\mu} = \{E_{\mathbf{p}} - V(\mathbf{p}), \mathbf{p}\}$ . Equation (A2) is evaluated numerically. The phenomenological self-energies  $[V(\mathbf{p}), S(\mathbf{p})]$  are fitted to polynomials in  $\mathbf{p}$ . Finally, the angle integration of the  $\delta$  function restricts the momentum integration so that  $|\cos\theta| \leq 1$ . The form factors  $F_1^i$  and  $F_2^i$  are taken from Ref. [14].

- 
- [1] H. Kurasaw and T. Suzuki, Nucl. Phys. **A490**, 571 (1988).
  - [2] K. Wehrberger and F. Beck, Phys. Rev. C **37**, 1148 (1988).
  - [3] C. J. Horowitz and J. Piekarewicz, Phys. Rev. Lett. **62**, 391 (1989); Nucl. Phys. **A511**, 461 (1990).
  - [4] J. P. Chen *et al.*, Phys. Rev. Lett. **66**, 1283 (1991).
  - [5] E. D. Cooper, S. Hama, B. C. Clark, and R. L. Mercer, Phys. Rev. C **47** 297 (1993).
  - [6] B. C. Clark, S. Hama, and R. L. Mercer, in *The Interaction Between Medium Energy Nucleons in Nuclei (Indiana Cyclotron Facility, Bloomington, Indiana)*, Proceedings of the Workshop on the Interactions Between Medium Energy Nucleons in Nuclei, edited by H. O. Meyer, AIP Conf. Proc. No. 97 (AIP, New York, 1983).
  - [7] C. J. Horowitz and B. D. Serot, Nucl. Phys. **A464**, 613 (1987).
  - [8] M. R. Ansatasio, L. S. Celenza, W. S. Pong, and C. M. Shakin, Phys. Rep. **100**, 327 (1983); R. Machleidt, in *Advances in Nuclear Physics*, edited by J. W. Negele and E. Vogt (Plenum, New York, 1986), Vol. 19, p. 189; G. Q. Li, R. Machleidt, and Y. Z. Zhuo Phys. Rev. C **48**, 1062 (1993); B. Ter Haar and R. Malfiet, Phys. Rep. **149**, 207 (1987).
  - [9] M. R. Frank, Phys. Rev. C **49**, 555 (1994).
  - [10] C. J. Horowitz and B. D. Serot, Nucl. Phys. **A368**, 503 (1981).
  - [11] M. J. Dekker, P. J. Brussaard, and J. A. Tjon, Phys. Lett. B **289**, 255 (1992); M. J. Dekker, P. J. Brussaard, and J. A. Tjon, Phys. Rev. C **49**, 2650 (1994).
  - [12] P. Barreau *et al.*, Nucl. Phys. **A402**, 515 (1983).
  - [13] Z. E. Meziani *et al.*, Phys. Rev. Lett. **52**, 2130 (1984).
  - [14] M. J. Musolf and T. W. Donnelly, Nucl. Phys. **A546**, 509 (1992).